Comparison of uncertainties in land-use change fluxes from bookkeeping model parameterization

Ana Bastos[1,2], Kerstin Hartung[1,3], Tobias B. Nützel[1], Julia E.M.S. Nabel[4], Richard A. Houghton[5], Julia Pongratz[1,4]

5   [1]Department of Geography, Ludwig Maximilian University of Munich, 80333 Munich, Germany
[2]Max Planck Institute for Biogeochemistry, Department of Biogeochemical Integration, 07745 Jena, Germany
[3]Now at: Deutsches Zentrum für Luft- und Raumfahrt, Institut für Physik der Atmosphäre, Oberpfaffenhofen, Germany
[4]Max Planck Institute for Meteorology, 20146 Hamburg, Germany
[5]Woodwell Climate Research Center, Falmouth, 02540, USA

10   *Correspondence to*: Ana Bastos (abastos@bgc-jena.mpg.de)

Abstract. Fluxes from deforestation, changes in land-cover, land-use and management practices (F_{LUC} for simplicity) contributed to circa 14% of anthropogenic CO_2 emissions in 2009-2018. Estimating F_{LUC} accurately in space and in time remains, however, challenging, due to multiple sources of uncertainty in the calculation of these fluxes. This uncertainty, in turn, is propagated to global and regional carbon budget estimates, hindering the compilation of a consistent carbon budget

15   and preventing us from constraining other terms, such as the natural land sink. Uncertainties in F_{LUC} estimates arise from many different sources, including differences in model structure (e.g., process- based vs. bookkeeping) and model parameterization. Quantifying the uncertainties from each source requires controlled simulations to separate their effects.

Here we analyze differences between the two bookkeeping models used regularly in the global carbon budget estimates since 2017: the model by Hansis et al. (Hansis et al., 2015) (**BLUE**) and that by Houghton and Nassikas (Houghton and Nassikas,

20   2017) (**HN2017**). The two models have a very similar structure and philosophy, but differ significantly both with respect to F_{LUC} intensity and spatio-temporal variability. This is due to differences in the land-use forcing, but also in the model parameterization.

We find that the larger emissions in **BLUE** compared to **HN2017** are largely due to differences in C densities between natural and managed vegetation or primary and secondary vegetation, and higher allocation of cleared and harvested material to fast

25   turnover pools in **BLUE** than in **HN2017**. Besides parameterization and the use of different forcing, other model assumptions cause differences, in particular that **BLUE** represents gross transitions which leads to overall higher carbon losses that are also more quickly realized than **HN2017**.

1 Introduction

Changes in land-use and management are estimated to have contributed to a global source of CO_2 to the atmosphere from the

30   pre-industrial period until the present, and to account for more than 10% of the total CO_2 emissions over the past decade according to the Global Carbon Budget 2019 (Friedlingstein et al., 2019). Fluxes from land-use change and management (F_{LUC}) result from changes in vegetation and soil carbon stocks and product pools due to human activities, such as

deforestation, forest degradation, afforestation and reforestation, as well as management practices such as wood harvest and shifting cultivation (rotation cycle between forest and agriculture), and subsequent regrowth of natural vegetation following

35 harvest or agricultural abandonment.

Reconstructing these changes consistently over the globe for the past centuries let alone millennia is, however, challenging and associated with high uncertainties (Hurtt et al., 2020; Klein Goldewijk et al., 2017; Pongratz et al., 2014; Ramankutty and Foley, 1999). This uncertainty in forcing translates directly to uncertainties in F_{LUC} estimates (Gasser et al., 2020; Pongratz et al., 2009; Stocker et al., 2011). Moreover, differences in definitions, terminology and on how indirect environmental effects

40 such as increasing atmospheric CO_2 concentration are considered, lead to large differences in F_{LUC} estimated by different methods (Gasser and Ciais, 2013; Grassi et al., 2018; Pongratz et al., 2014; Stocker and Joos, 2015). Grassi et al. (2018) have shown that by harmonizing definitions of managed land, estimates of F_{LUC} by a bookkeeping (BK) model, dynamic global vegetation models (DGVMs) and national inventories can be in part reconciled. The indirect environmental effects (accounted for in DGVMs but not in BK models) can be calculated by factorial simulations, in order to compare estimates from these two

45 methods (Bastos et al., 2020). Whether and how these indirect effects are accounted for in F_{LUC} creates large differences between estimates, but can be resolved by a consistent terminology (Grassi et al., 2018; Pongratz et al., 2014). Besides uncertainty in historical LUC areas and terminological issues, studies also differ with respect to which LUC practices are considered. Several studies have shown that including management practices such as shifting cultivation, crop or wood harvesting might increase F_{LUC} by 70% or more in individual DGVM estimates (Arneth et al., 2017; Pugh et al., 2015) with

50 management processes explaining some of the differences between biospheric fluxes from DGVMs and top-down estimates (Bastos et al., 2020).

In the Global Carbon Budgets since 2017 (Friedlingstein et al., 2019; Le Quéré et al., 2018b, a) F_{LUC} estimates for recent decades are taken as the mean of the estimates of two BK models, the one from (Houghton and Nassikas, 2017)) (**HN2017**) and the **BLUE** model described in (Hansis et al., 2015). However, even for these similar methods, estimates differ considerably

55 (Bastos et al., 2020; Friedlingstein et al., 2019). Cumulative F_{LUC} from 1850 until the present-day by these two BK models is 205±60PgC in the Global Carbon Budget 2019 (Friedlingstein et al. (2019), GCB2019 in the following). The F_{LUC} uncertainty after 1959 has been defined by best value judgement that there is a 68% likelihood that actual F_{LUC} lies within ±0.7PgC.yr^{-1} of the two models' mean and for earlier periods, the standard deviation of a group of DGVMs was used. This uncertainty range reflects uncertainties in parameterizations of the BK models, in the applied land-use change forcings as well as definitions,

60 processes considered, and is large enough to encompass the two models' estimates.

Besides differences in cumulative F_{LUC}, **BLUE** and **HN2017** also show very different temporal behaviors (Friedlingstein et al. (2019) and see Fig. 2 below). Noteworthy is an increase in F_{LUC} in **BLUE** but decrease in **HN2017** in the 1950s, which is likely attributable to the change in methodology in HYDE (Klein Goldewijk et al., 2017) from using FAOSTAT (FAOSTAT, 2015) estimates to population-based extrapolation in the past (Bastos et al., 2016). This comes on top of a generally steeper

65 increase in F_{LUC} in **BLUE** in 1870-1950. A second notable difference in temporal dynamics can be observed in the 2000s, as

has been shown by Bastos et al. (2020). Here, **BLUE** shows a strong increasing trend starting 2000, while **HN2017** estimates start decreasing after the late 1990s.

The estimated uncertainty of F_{LUC} in the Global Carbon Budgets is, thus, ca. 0.7 PgC.yr^{-1} or approximately +-50% of the average value, substantially larger than that of fossil fuel emissions. This uncertainty, in turn, is propagated to global and

70   regional carbon budget estimates, and affects the land sink term, which has often been quantified as residual depending on F_{LUC}. Houghton (2020) further noted that while net F_{LUC} can be constrained by the global carbon budgets, the component gross fluxes (sources such as deforestation and sinks, e.g. by afforestation) are even more uncertain.

Differences in initial land-cover distribution and transitions across different forcing datasets can also lead to substantial differences in estimated F_{LUC} (Vittorio et al., 2020; Li et al., 2018; Gasser et al., 2020). A detailed analysis of the impact of the

75   forcing datasets on LUC estimated by the OSCAR BK model has been performed by Gasser et al. (2020), and Hartung et al. (2021) analyzed the effect of the different LUC from LUH2v2.1 (Hurtt et al., 2020) and of various internal model assumptions in **BLUE** on F_{LUC}.

Despite the relevance of the **BLUE** and **HN2017** estimates for the global carbon budget analyses, stark discrepancies between these two models (Friedlingstein et al., 2019) and the long-standing appreciation of various factors contributing to such

80   differences (Hansis et al., 2015; Houghton et al., 2012), no quantitative analysis on the contribution of model differences to this discrepancy has so far been performed. Both models rely on observation-based estimates for their parameterizations and forcing datasets and the choices on spatial and plant-functional type representation, starting year and other aspects are well justified in both models. However, these multiple differences add to uncertainty in F_{LUC} estimates and make it difficult to attribute differences in F_{LUC} and their trends to specific aspects of the F_{LUC} calculation.

85   In this study, we fill this gap and assess to which extent the different parameterizations in **BLUE** and **HN** affect global and regional F_{LUC} estimates and their trends. We further investigate the effect of the different parameter choices on the gross LUC fluxes.

2 Data and Methods

2.1 Model characteristics and datasets used

90   In this study we focus on the two BK models used in the GBC2019 as well as in the Intergovernmental Panel on Climate Change's Special Report on Climate Change and Land (Shukla et al., 2019) to estimate F_{LUC}: the Bookkeeping of Land-Use change Emissions model, **BLUE** (Hansis et al., 2015) and the model from Houghton and Nassikas (2017), which is referred to as **HN2017**.

The two models differ in several aspects, the most relevant ones summarized in Table 1. An important difference, which we

95   will account for in this study, is that **BLUE** estimates F_{LUC} from gross LUC transitions, while **HN2017** uses net transitions. Gross transitions resolve that within a unit (grid-cell for BLUE, country/region for **HN2017**) there may be concurrent back- and forth-transitions between a pair of land-use types, for example 30% of the unit area may be transformed from forest to

cropland, while on 20% cropland is abandoned and forest regrows. Net transitions would represent this as a 10% forest to cropland transition. These sub-unit changes are particularly important for large units (large grid-cells or country-level, (Wilkenskjeld et al., 2014)) and in regions where shifting cultivation prevails (in particular in the tropics; (Heinimann et al., 2017)) or with small-scale dynamics such as in Europe (Fuchs et al., 2015). **HN2017** implicitly includes shifting-cultivation effects if these are captured by FAO (2015) data and allows degraded lands start to accumulate carbon again after 10 years of no change. The two models are also forced by distinct LUC datasets: **HN2017** calculated F_{LUC} at country-level based on statistics of changes in croplands and pastures extent since 1961 and harvest data and changes in forests and other land since 1990 (FAO, 2015; FAOSTAT, 2015), with extrapolations to earlier time periods. **BLUE**, on the other hand, is forced by spatially explicit transitions and harvest at 0.25x0.25 degree resolution from the Land-Use Harmonization dataset (LUH2v2.1) (Friedlingstein et al., 2019; Hurtt et al., 2020). LUH2v2.1 calculates cropland, pasture, urban, and ice/water fractions between 850 and 2018 based on the HYDE3.1 dataset (Klein Goldewijk et al., 2017). HYDE3.1 in turn, also used FAOSTAT (2015) data for country-level agricultural areas (cropland, pasture, rangelands) data after 1961, extrapolated backwards in time using total population and agricultural area per-capita ratios for each country. The cropland and forest area estimates from these two different datasets (LUH2v2.1vs. FAO) differ considerably in several key LUC areas, for example South America and SE Asia (Li et al., 2018), which can lead to large differences in F_{LUC} and their trends found in those regions (Bastos et al., 2020; Vittorio et al., 2020).

Following a transition, C stocks in the different pools will decay following response curves with characteristic decay times (fast for biomass pools and slow for soil pools). To estimate changes in C stocks, the models rely on values of C density in above and below-ground pools which are PFT-specific and based on measurements (Table A2). However, the models differ in the number of plant functional types (Table A1) and their spatial distribution (per country in **HN2017** and spatially explicit in **BLUE**).

For harvest and clearing, the dislocated C is distributed between a dead soil pool and three product pools of different lifetimes, 1-, 10- and 100-yr (Table A3). In the case of BLUE these fractions are fixed and PFT-specific, while **HN2017** distinguishes between harvested wood use over time (fuel, 1-yr, industrial, 10 and 100-yr time-scales), so that the fraction allocated to each pool changes over time.

Parameters in **BLUE** and **HN2017** are defined on a PFT basis, but **HN2017** distinguishes 20 PFTs (3 of them desert PFTs), while **BLUE** distinguishes 11 PFTs. In order to compare the parameterizations, the different PFTs need to be mapped. Most **HN2017** PFTs can be aggregated into the often more broadly-defined **BLUE** PFTs but some of the PFTs in **BLUE** do not correspond to **HN2017** PFTs (e.g., summer-green shrubs) (Table A1). A map of the PFT distribution from **HN2017** is not available, as the PFT fractions are defined on a per country basis. When aggregated globally, the values of BLUE and HN2017 show good agreement in the global extent of croplands (15.3Mkm^2 and 13.8Mkm^2 for **HN2017** and **BLUE**, respectively, in 2015) and forests (39.9Mkm^2 and 40.9Mkm^2 for **HN2017** and **BLUE**, respectively, in 2015) .

130   When more than one PFT class from **HN2017** is aggregated to one PFT in **BLUE**, we estimate the corresponding parameter

value as the average value weighted by the **HN2017** PFT fractions within that country. We use therefore spatially explicit

values in the model simulations (as in Fig. A1), but they are summarized as spatially-averaged values in Table A1 .

Table 1 – Summary of the most important characteristics of the two F_{LUC} estimates from the two BK models used in the GCB2019 (BLUE and HN2017), including how F_{LUC} is calculated in the standard version and configuration of each model, the processes
135 **represented and how they are parameterized. The model assumptions and parameterizations investigated in this study (see Table 2) are highlighted in bold.**

		BLUE	HN2017
F_{LUC} calculation	Spatial representation	Grid scale (0.25°x0.25°)	Country/region level
	PFTs	11 spatially-explicit	20 per country
	LUC transitions	**Gross**	**Net**
	Starting year	**850**	**1700**
	Last year	2018	2015
	Response curves	Exponential	Exponential
	LUC transitions	LUH2v2h (Hurtt et al., 2020)	(FAO, 2015; FAOSTAT, 2015)
Processes	Shifting cultivation	Included explicitly	Indirectly included (if FRA forest loss is larger than FAO agricultural expansion)
	Harvest	3 Pools (1, 10, 100 years)	3 Pools (1, 10, 100 years)
	Clearing	3 Pools (1, 10, 100 years) plus slash	3 Pools (1, 10, 100 years) plus slash
Parameters	Carbon densities (**Cdens**)	For each of the 11 PFTs (vegetation and soil) based on (Houghton et al., 1983)	Per country and for each of the 20 PFTs (vegetation); only per PFT (soil)
	Decay times for the response curves (**RCt**)	For each of the 11 PFTs	For each of the 20 PFTs
	Pool allocation fractions (**Alloc**)	Different allocation fractions for each of the 11 PFTs	Different allocation fractions per country and for each of the 20 PFTs

2.2 Factorial Simulations

140   In order to attribute differences in F_{LUC} between the two models to specific aspects from Table 1, we perform a set of factorial simulations with **BLUE** (see Table 2), in which we replace the BLUE parameters with those from **HN2017** (see also schematic in Figure 1). We then compare these simulations with the fluxes estimated by HN2017, published in (Houghton and Nassikas, 2017; Friedlingstein et al., 2019).
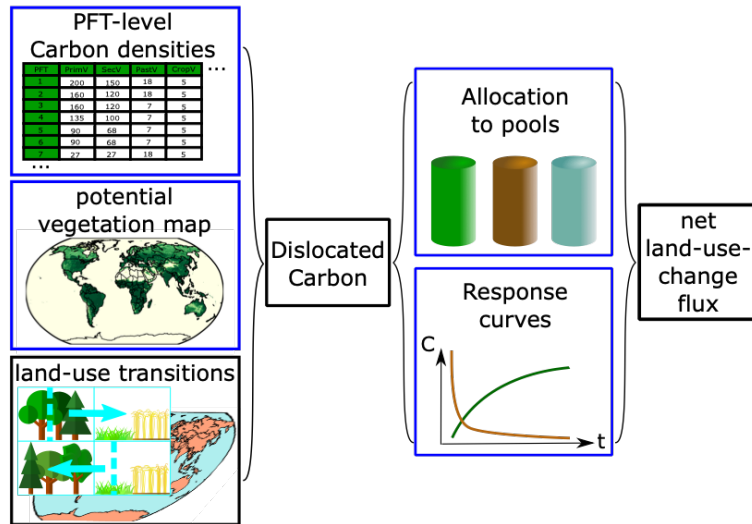
145   **Figure 1. Schematic description of the BLUE model set up and of the changes made in each of the factorial simulations (highlighted in blue boxes and summarized in Table 2). The model is forced by a map of gridcell-level land-use transitions occurring at time t (gross vs net). These are then combined with a potential vegetation map of 11 natural vegetation types (Table A1), each having specific carbon densities in vegetation and soil pools (Cdens), to calculate the carbon dislocated by each transition. The mass of dislocated carbon is then distributed among different slash and product pools (Alloc), with specific response curves with different**
150   **decay times (t).**

The different simulations performed, and their justification are as follows (summarized in Table 2):

- **S_{BL}**: the **BLUE** simulation performed for GCB2019, following the set up described in Table 1, i.e., the standard BLUE configuration

- **S_{BL-Net} (reference simulation)**: the **BLUE** simulation as **S_{BL}** but starting in 1700 and using net transitions rather than
155   gross transitions. The difference to **S_{BL}** provides an estimate of the impact of the core setup of **HN2017** (net transitions and starting in 1700). In this simulation, net land conversion is taken first from primary land, i.e. abandonment (to secondary land) is allowed to cancel clearing from preferentially primary land in addition to secondary land, which reduces emission estimates more than if abandonment were allowed to cancel clearing only of secondary land (Hansis et al., 2015). The choice for net transition implementation aims to make F_{LUC} estimates more comparable to the
160   approach in **HN2017,** albeit keeping the different original forcing (LUH2v2.1 in **BLUE** as compared to FAO in **HN2017**). All subsequent simulations are run with this setup, but with different parameterizations (Table 2).

- **S$_{HNCdens}$**: in this simulation, **BLUE** is run using the C densities in vegetation and soil parameters from **HN2017**. Although C density parameters in **HN2017** are defined on a per country and per PFT basis, only vegetation C densities differ between countries for a given PFT, while soil C densities only differ per PFT (example for tropical evergreen broadleaved forest in Figure A1). The global average values per PFT for **BLUE** and **HN2017** are given in Table A2. **BLUE** has generally higher vegetation and soil C densities in the tropics and most temperate PFTs, and lower vegetation and soil C densities in pastures, and lower soil C densities in croplands, compared to the average values of **HN2017**.

- **S$_{HNAlloc}$**: in this simulation, **BLUE** is run using the harvest and clearing allocation fractions, and the slash fractions following clearing from **HN2017** but the C densities in vegetation and soil from **BLUE**. The global average values for **BLUE** and **HN2017** are given in Table A3. In the actual HN2017 model run (Houghton and Nassikas, 2017), the allocations vary over time. Since BLUE uses temporally static fractions, we used an average over the full period (1850-2015). Harvest slash fractions in BLUE (with time-scales of 5-15 years in BLUE) are larger in BLUE than in **HN2017** for all PFTs. **HN2017** allocates more harvest product to the long-lived pool over the period 1850-2015 than BLUE (Table A3). For clearing, the short and long-lived pools are relatively similar between the models but the medium-lived pool is larger in BLUE, depending however on the PFT considered. The slash fractions following clearing from **HN2017** are also used instead of those in **BLUE**.

- **S$_{HNt}$**: the decay times from **HN2017** are used in **BLUE**..

- **S$_{HNFull}$**: **BLUE** is run using net LUC transitions, starting in 1700 and using **HN2017** parameters for C densities, harvest and clearing allocation fractions and decay times (i.e., a combination of S$_{HNCdens}$, S$_{HNAlloc}$ and S$_{HNt}$).

Table 2: Selected settings in the simulations conducted with BLUE. The row in bold highlights the reference simulation.

	Starting year	Transitions	C densities (Cdens)	Carbon allocation (Alloc)	Response curves decay times (t)
S$_{BL}$	850	Gross	BLUE	BLUE	BLUE
S$_{BL-Net}$	**1700**	**Net**	**BLUE**	**BLUE**	**BLUE**
S$_{HNCdens}$	1700	Net	HN2017	BLUE	BLUE
S$_{HNAlloc}$	1700	Net	BLUE	HN2017	BLUE
S$_{HNt}$	1700	Net	BLUE	BLUE	HN2017
S$_{HNFull}$	1700	Net	HN2017	HN2017	HN2017

In those simulations where **BLUE** is run with all or a sub-set of **HN2017** parameters (S$_{HNCdens}$, S$_{HNAlloc}$, S$_{HNt}$), instead of global values per PFT, the values per PFT from **HN2017** are translated into **BLUE** PFTs and organized into parameter maps that can be read by **BLUE**. The difference between these simulations and S$_{BL-NET}$ provides an estimate of F_{LUC} differences each

including one set of parameters from **HN2017** in **BLUE**. For S_{HNFull}, the difference with $S_{BL\text{-}NET}$ is not expected to be simply the sum of the corresponding $S_{HNCdens}$, $S_{HNAlloc}$, S_{HNt} differences because of interactions between C densities, allocation fractions and response times, with differences in model structure and LUC forcing, as described in Figure 1.

2.3 Model comparison

We calculate F_{LUC} from the different simulations between 1850 and 2015 (the period common to both datasets) for the globe and for the 18 regions used in (Bastos et al., 2020) to evaluate sources of uncertainty in land carbon budgets: Canada (CAN), USA, central America (CAM), northern South America (NAM), Brazil (BRA), southern South America (SSA), Europe (EU), northern Africa (NAF), equatorial Africa (EQAF), southern Africa (SAF), middle east (MIDE), Russia (RUS), Korea and Japan (KAJ), central Asia (CAS), China (CHN), southern Asia (SAS), SE Asia (SEAS) and Oceania (OCE). We then evaluate separately the contribution of running **BLUE** with the reference **HN2017** setup i.e., with net instead of gross transitions and starting in 1700s ($S_{BL\text{-}Net}$ - S_{BL}). $S_{BL\text{-}Net}$ is then used as the baseline for comparison with other simulations, which follow the same setup (net emissions in simulations starting in 1700).

Both **BLUE** and **HN2017** add emissions from peat burning (Van Der Werf et al., 2017) and drainage (Hooijer et al., 2010) in a postprocessing step. For easier comparison of direct model output, we do not include these post-processing steps.

For all simulations, we compare both the interannual variability in F_{LUC} and the resulting cumulative emissions between 1850 and 2015. The discrepancies in interannual variability of estimated F_{LUC} between HN2017 and each simulation from BLUE (S_i) are assessed by the root mean square difference of F_{LUC} from each simulation, calculated as:

$$RMSD_{HN-BLUE-i} = \sqrt{\frac{\sum_i^N (HN2017_i - S_i)^2}{N}} \qquad \text{Eq. (1)}$$

where N is the number of years. In addition, we compare the effect of the different parameterizations on the gross LUC fluxes: fluxes from clearing of primary or secondary natural vegetation, wood harvest (net of decay and regrowth), abandonment of agricultural land (cropland and pasture) and transitions between cropland and pasture.

3 Results

3.1 Global F_{LUC}

We analyze annual F_{LUC} from 1850 until 2015 (Figure 2, left panel). The **BLUE** simulation for GCB2019 (S_{BL}, dark blue line) estimates higher emissions from LUC than **HN2017** (black line). The cumulative emissions between 1850-2015 (Figure 2, right panel) are 139PgC for **HN2017** and 245PgC for S_{BL}. $S_{BL\text{-}Net}$ shows lower F_{LUC}, but results in cumulative emissions only ca. 13% lower (214PgC) than when using gross transitions. As in previous **BLUE** estimates, both S_{BL} and $S_{BL\text{-}Net}$ show an increase in F_{LUC} from 1850 until the mid-20th century, peaking at around 1960 and then decreasing sharply until the 1990s, while **HN2017** shows less variability. The two datasets further show contrasting trends from around 1975 until 2015, with **BLUE** increasing sharply after the late 1990s, when **HN2017** shows a decrease.

All **BLUE** simulations show similar interannual variability patterns, consistent with the use of the LUH2v2.1 forcing, but these variations are dampened when the parameters for C densities, allocation fractions and time constants from HN are used. The **BLUE** simulation using the full set of **HN2017** parameters (S_{HNFull}) shows F_{LUC} close to those of **HN2017** until the 1980s and

220 with a weak peak in emissions in 1960s and relatively stable F_{LUC} rather than an increasing trend in 2000-2015. The resulting cumulative F_{LUC} for S_{HNFull} is 104PgC, 52% lower than S_{BL-NET}, at the low end of previous estimates (Hansis et al., 2015; Houghton et al., 2012). This value is substantially outside the cumulative budget range of the GCB2019 (205 ± 60 PgC 1850-2018), but still consistent with the uncertainty range of ±0.7 PgC.yr⁻¹ provided by GCB2019 after 1959.
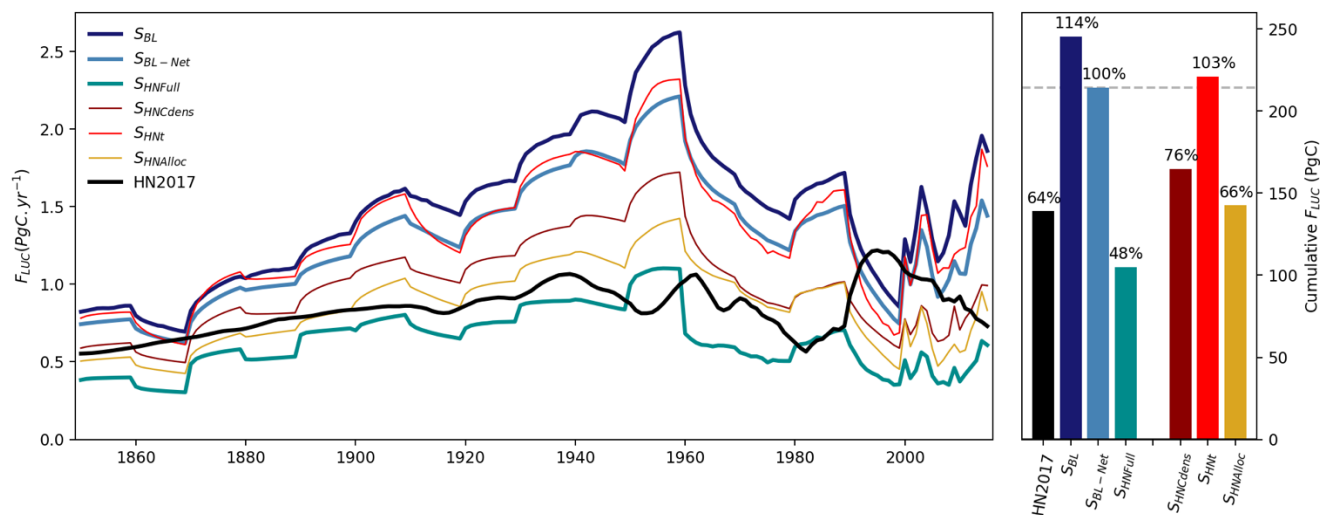
225 **Figure 2.** Global F_{LUC} between 1850 and 2015 (A) from the two bookkeeping model estimates in GCB2019 (HN2017 in black and S_{BL} for BLUE in dark blue), the BLUE simulations with net LUC transitions and standard BLUE parameterization (light blue, S_{BL-Net}, used as reference for all subsequent BLUE runs) and using all tested HN2017 parameterizations together (cyan, S_{HNFull}). The factorial simulations with only one set of parameters changed are shown in thin lines ($S_{HNCdens}$ in dark red, S_{HNt} in red, $S_{HNAlloc}$ in yellow). The corresponding cumulative totals between 1850 and 2015 are shown in the panel B, and values relative to S_{BL-Net} are shown by the
230 numbers above bars.

The parameters that lead to larger differences in global F_{LUC} are the C densities ($S_{HNCdens}$, Figure 2 dark red) and the allocation rules ($S_{HNAlloc}$, yellow), while changing the decay times have small effect. Both $S_{HNCdens}$ and $S_{HNAlloc}$ result in lower F_{LUC} over the 1850-2015 period, and weaker increasing trends between 2000 and 2015, which indicates that the trends in this period are not only due to forcing differences (Bastos et al., 2020), but in part from model parameterization. The cumulative F_{LUC} in

235 1850-2015 is 164 PgC and 142PgC for $S_{HNCdens}$ and $S_{HNAlloc}$ respectively i.e., 24% and 34% lower than S_{BL-Net}, and closer to the **HN2017** estimate on global scale. The lower F_{LUC} with **HN2017** C densities can be explained by the **HN2017** lower C densities in both vegetation and soil for most PFTs and the smaller difference between primary and secondary forest C stocks (Table A2) compared to **BLUE**. In particular, **BLUE** often features higher vegetation carbon in broadleaf forests and higher soil carbon in most other ecosystems than **HN2017**, which, together with lower soil carbon assumed for cropland and pasture,

240 leads to substantially larger carbon losses in BLUE for many transitions (Table A2). Even though S_{HNt} results in a small positive

difference in cumulative F_{LUC} relative to S_{BL-NET} (221 PgC), effect of response curve times is multiplicative (Figure 1), therefore the F_{LUC} trends are amplified (Figure 2, left panel).

3.2 Regional patterns

The global differences between simulations result from interactions between the different factors and in the types of LUC occurring in a given point in space and time. We first analyze the temporal evolution of regional F_{LUC} for each simulation (Figure 3).
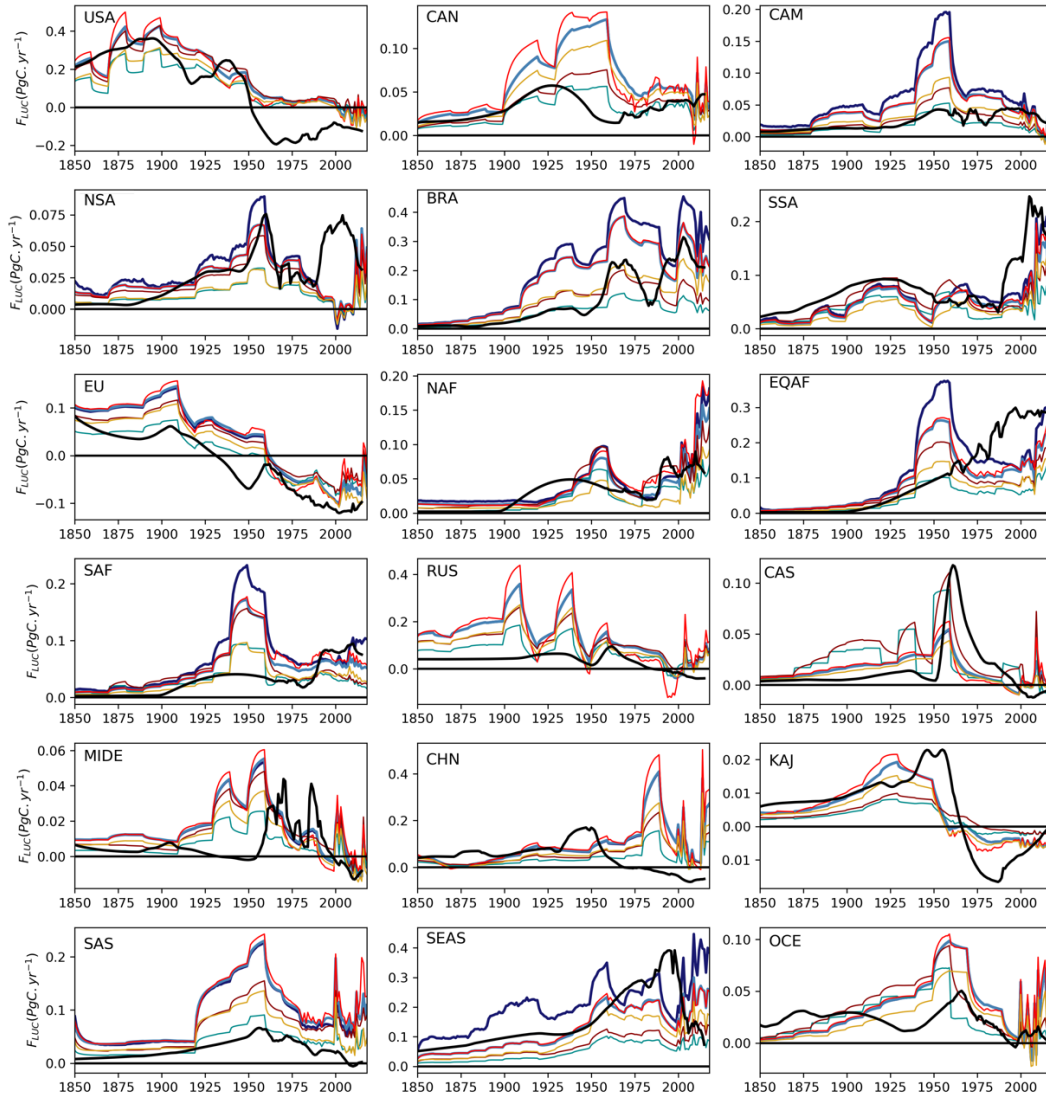
Figure 3. Regional F_{LUC} between 1850 and 2015 from the two BK model estimates in GCB2019 (HN2017 in black and S_{BL} for BLUE in dark blue), the BLUE simulations with net LUC transitions and standard parameterization (light blue, S_{BL-Net}) and using HN2017 parameterizations (cyan, S_{HNFull}). The factorial simulations with only one set of parameters changed are shown in thin lines ($S_{HNCdens}$ in dark red, S_{HNt} in red, $S_{HNAlloc}$ in yellow).

The factorial analysis sheds light on the underlying reasons of the diverging trends in the 2000s, where **BLUE** showed an upward trend, opposing downward trend in F_{LUC} from **HN2017**. In absolute terms, the upward trend in **BLUE** stems foremost from BRA (a peak of about 0.45 PgC.yr^{-1} in the early 2000s, then a decline; similar in **HN2017**, but peaking at about 0.3 PgC.yr^{-1}), SSA (also captured by **HN2017**, but accelerating from the 2000s to the 2010s in **BLUE**, decelerating in **HN2017**), NAF (by comparison more stable in **HN2017**), EQAF (similar values as in **HN2017**, but with 0.15 PgC.yr^{-1} F_{LUC} in **BLUE** in the 1970s-2000s is only about half that of **HN2017**) and SEAS (where **HN2017** has a peak in the 1990s, then a steep drop of 0.3 PgC.yr^{-1} to 2015, while **BLUE** F_{LUC} picks up by about 0.2 PgC.yr^{-1} over the 2000s). Additionally, **BLUE** shows an increase in F_{LUC} in CHN for the 2010s, while **HN2017** estimates a sink due to afforestation. In all of these regions, adjusting **BLUE** partly or fully to **HN2017** parameters does not obviously bring trends closer together, because a lowering of the 2000s F_{LUC} in **BLUE**, which results from several of the factorial experiments, would lead to lower F_{LUC} in earlier time periods as well.

To summarize these patterns, we calculate the relative average differences in regional cumulative F_{LUC} from S_{BL-Net} and S_{HNFull} with S_{BL} (top panel of Figure 4 A, values in % change) and the root mean square difference to **HN2017 (Eq. 1,** RMSD$_{HN-BLUE}$**),** which reflects differences in interannual variability (top panel of Figure 4B, in TgC.yr^{-1}).

Even though S_{BL-Net} results in a small (-13%) decrease in global F_{LUC} compared to S_{BL} as discussed above, regional differences show stronger decreases, especially in regions with intensive shifting cultivation practices, such as SEAS (-40%), CAM (-22%), SAF and EQAF (-23% in both). S_{BL-Net} additionally leads to higher agreement in interannual variability with **HN2017** () at global scale, but also for most regions (i.e., lower RMSD$_{HN-BLUE}$, Figure 4B). Europe shows 7% higher cumulative F_{LUC} for S_{BL-Net} than S_{BL}, likely because of the importance of sub-pixel post-abandonment recovery and re-/afforestation dynamics in Europe (Bayer et al., 2017; Fuchs et al., 2015). However, this increases the RMSD$_{HN-BLUE}$ by only 2TgC.yr^{-1}.

As seen for global F_{LUC}, the simulation using HN parameter values (S_{HNFull}) leads to a reduction of F_{LUC} by 50% or more compared to S_{BL} in many regions (dark blue colors, see values in the center of grid cells in Figure 4A), except for central Asia (CAS), where an increase of 47% is estimated, mainly due to differences in C density parameters. The reductions in cumulative F_{LUC} differences in CAM, BRA, EU and SEAS. Decreases in the RMSD$_{HN-BLUE}$ between S_{HNFull} and S_{BL-Net} globally and for11 of the 18 regions (Figure 4B), with small increases elsewhere. This shows that differences in setup and parameterization cancel differences arising from the different land-use forcing in **BLUE** and **HN2017** in some regions. In addition, the reductions in RMSD$_{HN-BLUE}$ in S_{HNFull} compared to S_{BL} are stronger than for S_{BL-Net}, indicating that parameterization differences have stronger contribution to RMSD$_{HN-BLUE}$ than the impact of simulation net/gross transitions.
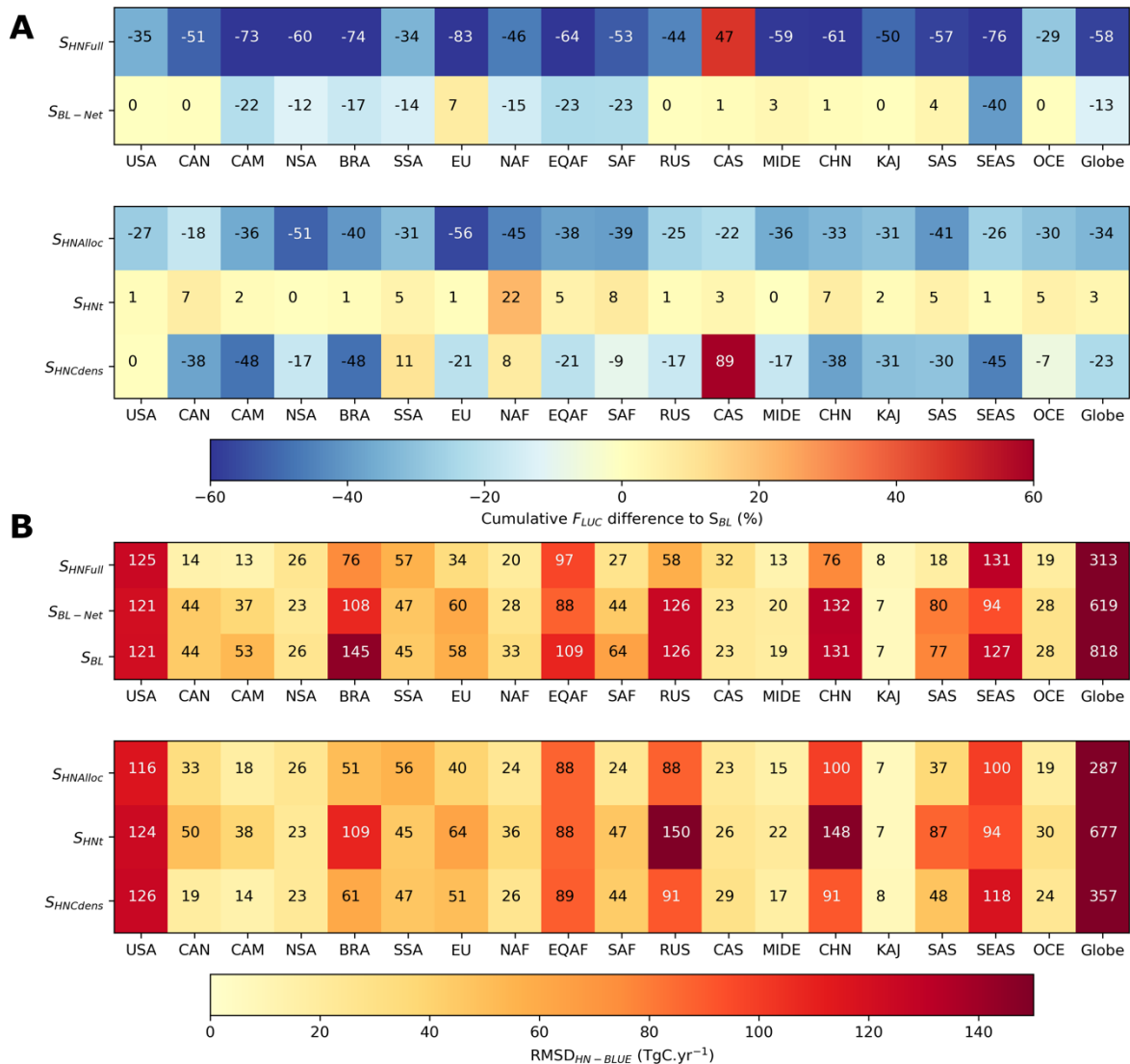
Figure 4. (A) Relative changes in cumulative simulated F_{LUC} between 1850-2015 for each region for S_{BL-Net} and S_{HNFull} compared to S_{BL} (top two rows) and the relative effect of each parameter change, compared to S_{BL-NET} (bottom three rows) indicated by the colors and numbers in the center of cells. **(B)** The RMSD$_{HN-BLUE}$ for each simulation indicated by the colors and numbers in the center of cells. All panels show results for the period 1850–2015.

The differences between S_{BL-Net} and each of the factorial simulations (bottom panel of Fig. 4A) shows that C densities and allocation rules are the dominant factors not just for global F_{LUC}, but also in most regions, and lead to lower RMSD$_{HN-BLUE}$, compared to S_{BL-Net} (Figure 4B). Using **HN2017** allocation fractions to pools for harvest and clearing results in lower cumulative F_{LUC} everywhere ($S_{HNAlloc}$) and decreases the RMSD$_{HN-BLUE}$ at global scale and in all regions but NSA and SSA. Altering C densities ($S_{HNCdens}$) has contrasting effects in cumulative F_{LUC} between regions, increasing cumulative F_{LUC} in 3

out of 18 regions. Strong reductions in RMSD$_{HN-BLUE}$ for $\mathbf{S_{HNFull}}$ are found in in BRA, RUS, CHN and SAS (top panel Figure 4B), explained by RMSD$_{HN-BLUE}$ reductions by changing the C densities in vegetation and soil pools ($\mathbf{S_{HNCdens}}$) and allocation fractions. In SEAS, cumulative $\boldsymbol{F_{LUC}}$ is reduced when using **HN2017** parameters ($\mathbf{S_{HNFull}}$) but with a higher RMSD$_{HN-BLUE}$. In this region C density parameters contribute the most to the reduction of bias, compared to $\boldsymbol{S_{BL-Net}}$, and both C density parameters and allocation fractions contribute to the increase in RMSD$_{HN-BLUE}$. This highlights the importance of interactions between different parameters to the overall $\boldsymbol{F_{LUC}}$ variability. The decay times generally contribute to small increases in cumulative $\boldsymbol{F_{LUC}}$ compared to $\boldsymbol{S_{BL-Net}}$, except NAF where they increase $\boldsymbol{F_{LUC}}$ by 22%, and would slightly amplify RMSD$_{HN-BLUE}$ globally and in 13 of the 18 regions.

3.3 Effects on gross $\mathbf{F_{LUC}}$ component fluxes

To better understand the effects of the different parameterizations on $\boldsymbol{F_{LUC}}$, we analyze the spatial distribution of the differences between $\mathbf{S_{HNFull}}$, $\mathbf{S_{HNCdens}}$, $\mathbf{S_{HNAlloc}}$, $\mathbf{S_{HNt}}$ and $\boldsymbol{S_{BL-Net}}$ decomposed into gross $\boldsymbol{F_{LUC}}$: fluxes from harvest, clearing, abandonment/regrowth and transitions between crop and pasture (Figure 5).
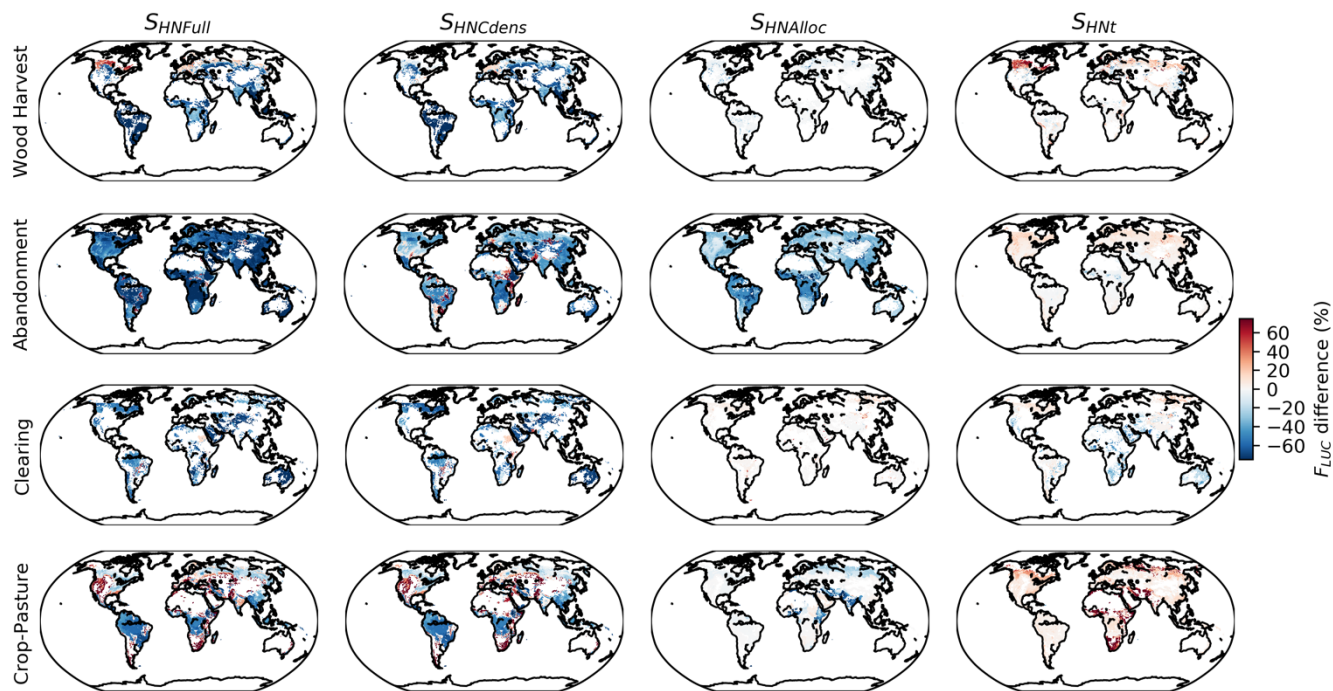
Figure 5. Spatial distribution of relative differences in average F_{LUC} between 1850-2018 for each of the four simulations with HN2017 parameters ($\mathbf{S_{HNFull}}$, $\mathbf{S_{HNCdens}}$, $\mathbf{S_{HNAlloc}}$, $\mathbf{S_{HNt}}$,), compared to S_{BL-Net} for different F_{LUC} components: wood-harvest, abandonment, clearing and crop-pasture transitions. Regions with average low values of F_{LUC} (e.g. deserts) are masked.

In most grid cells, the difference between $\mathbf{S_{HNFull}}$ and $\boldsymbol{S_{BL-Net}}$ is dominated by the effects of the parameterization of C densities in gross fluxes and allocation rules for abandonment fluxes. For $\boldsymbol{F_{LUC}}$ from abandonment and clearing to agriculture (crop and pasture) the differences are mostly negative (i.e., higher uptake from recovery and lower emissions from clearing to agriculture

using **HN2017** parameterization), while for the fluxes from transitions between crop and pastures and harvest, regional contrasts between positive and negative differences are found. The lower F_{LUC} from clearing to agriculture for S_{HNFull} in most grid cells is linked with the lower vegetation and soil C densities for most forest PFTs (Table A2). Higher F_{LUC} from wood harvest are simulated by S_{HNFull} in eastern and northern North America, central Europe and Scandinavia and China, mostly
315 related with response curve time-constants. Other transitions (crop to pasture or pasture to crop) result in higher F_{LUC} for S_{HNFull} in most semi-arid regions, which is explained to a larger extent by differences in C densities and time-constants between the two models ($S_{HNCdens}$, S_{HNt}) than by allocation rules ($S_{HNAlloc}$) (Table A2).

4 Discussion

Fluxes from land-use change and management are one of the most uncertain and least constrained components of the global
320 carbon cycle (Bastos et al., 2020; Friedlingstein et al., 2019; Houghton, 2020). Several sources of uncertainty in F_{LUC} have been previously analyzed, such as the choice of gross versus net LUC transitions (Bayer et al., 2017; Fuchs et al., 2015; Gasser et al., 2020; Wilkenskjeld et al., 2014) the definitions and terminology used (Grassi et al., 2018; Pongratz et al., 2014), or the management processes considered (Arneth et al., 2017; Pugh et al., 2015). The two bookkeeping models used in the Global Carbon Budgets may differ in their F_{LUC} estimates due to differences in the forcing data and differences in model structure,
325 parameterization and in how certain processes are represented. The impact of the LUC forcing on F_{LUC} has been extensively investigated in previous studies (Bastos et al., 2020; Gasser et al., 2020; Hartung et al., 2021). Both models have a similar structure (Table 2) and both models use parameters from different sources that are based on observations which are, however, uncertain. Here we evaluate how the different model parameterizations impact F_{LUC} estimates and whether they can explain differences in global and regional average F_{LUC} and on variability between the two models since 1850.
330 The simulation with net transition (S_{BL-Net}) reduces differences in the average and inter-annual variability of F_{LUC} estimates from **BLUE** and **HN2017**. The contribution of gross to F_{LUC} is smaller than previous estimates (15-38%, (Arneth et al., 2017; Fuchs et al., 2015; Hansis et al., 2015)) and also lower than in earlier **BLUE** simulations that used the same rule. Canceling of primary and secondary land clearing, with primary first, gave 24% lower emissions in Hansis et al. (2015). The differences are likely explained by the substantial changes that came in with the change from LUH1 to LUH2 versions, in particular the change
335 to Heinimann et al. (2017) shifting cultivation maps.
Based on observation-based constraints by atmospheric inversions Bastos et al. (2020) pointed out that F_{LUC} estimated by DGVMs and **BLUE** in BRA, SEAS, EU and EQAF were probably too high. Our analysis shows that F_{LUC} estimates for these regions except EU would be lower if the setup of **HN2017** were used i.e., starting in 1700 instead of AD 850 and using net transitions, and all four regions would show even larger reductions in F_{LUC} if the parameterization of **HN2017** were used in
340 **BLUE**. However, these changes would also bring down F_{LUC} estimates in many regions that were not deemed too high in F_{LUC} based on the constraint by observations. This suggests that neither **BLUE** nor **HN2017** setup and parameterization can be judged as being superior to the other for all regions of the world and all time periods.

The rules for allocation of displaced carbon to different pools have the strongest effect on average F_{LUC}, as well as their variability, followed by C density parameters. Contrary to C densities (Section 4.1), at the moment no global dataset of allocation parameters exists that could be compared to the allocation fractions used here. **BLUE** and **HN2017** F_{LUC} in 1850-2015 show better agreement in temporal variability, mostly because fact that the C density and allocation parameterizations of **HN2017** dampen the effect of differences in land-use change transitions.

This elimination of the 2000s trend difference in some regions comes at the cost of larger divergences in earlier times. With high LUC dynamics in the 20th century in some regions, which is more strongly captured by **BLUE** with its representation of gross transitions, slightly larger C density losses with the transformation of natural vegetation to agriculture or degradation by wood harvesting and rangelands may lead to an increase in F_{LUC} beyond what would be expected from net land-use areas alone. On top comes a distribution of cleared and harvested material to faster pools (more slash in **BLUE**, more long-lived products in **HN2017**), which also emphasizes the effects of LUC dynamics. The differences between **BLUE** and **HN2017** are thus a combination of higher LUC dynamics in **BLUE** (by using LUH2v2.1 and accounting for gross transitions), and of faster material decay than in **HN2017**. The different trends of **BLUE** and **HN2017** in the 1950s and after 1990 are instead largely attributable to the different LUC forcing (Gasser et al., 2020).

4.1 Constraining C densities

The parameterization of C densities of vegetation and soil pools is the second most relevant parameter, but one that affects all flux components. Even though both models were parameterized based on observation-based C densities, these parameters are highly uncertain, as they are derived from sparse plot-level data with high variance across datasets (Brown and Lugo, 1982; Post et al., 1982; Schlesinger, 1984; Zinke et al., 1986). Remote-sensing based estimates of potential vegetation C stocks in undisturbed lands and well as present-day C stocks have been produced by Erb et al. (Erb et al., 2018), including their uncertainty. The values of Erb et al. (2018) can, therefore, be compared to the potential C stocks simulated by **HN2017** and by **BLUE** using the different configurations in this study (circles in Figure 6), as well as of simulated present-day carbon stocks (small circles, end of arrows). In addition, we compare simulated C stocks with those of Anav et al. (2013) for the present day.
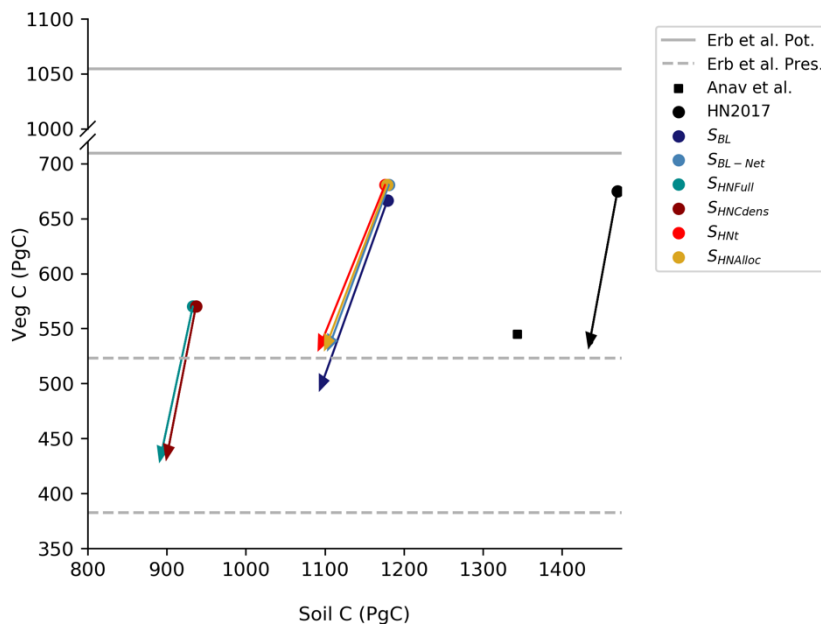
Figure 6. Carbon stocks in vegetation (yy-axis) and soils (xx-axis) simulated by BLUE for the pre-industrial period (1850, big circles) and present time (2018, small circles, end of arrows). These values are compared to two observation-based reference datasets: that of Anav et al. (2013) for both vegetation and soil carbon stocks (black square) and the upper and lower values of potential (solid lines) and present-day (dashed lines) carbon stocks in vegetation from Erb et al. (2018).

All BLUE simulations, as well as **HN2017**, have 4-6% lower potential C stocks in vegetation than estimates in Erb et al. (2018) (Figure 6). Since the values of potential biomass in Erb et al. were estimated for present day, they include the effect of environmental changes such as CO_2 fertilization, and are expected to be up to 10% higher than they would be without these effects (Pongratz et al., 2014). Therefore, the C stocks in vegetation simulated both by BLUE and HN2017 are consistent with these remote-sensing based estimates, if environmental effects are excluded. The methodology of using highest percentiles in a moving window as potential value in Erb et al. (2018) could overestimate biomass because it has a bias towards capturing oldest rather than average forests in a cycle of natural disturbances. Additionally, these simulations result in present-day C stocks in vegetation that are within the range provided by Erb et al. (2018), or close to its upper limit, and are also consistent with the reference value from Anav et al. (2013). All simulations estimate lower C stocks in the soil, compared to Anav et al. (2013). **HN2017** has higher C stocks in soil both for the pre-industrial period and present-day, compared to **BLUE** simulations, which are closed to the values estimated by Anav et al. (2013). The two simulations using **HN2017** carbon densities (S_{HNFull}, and $S_{HNCdens}$) result in too low C stocks in soils, compared to Anav et al. (2013), and much lower potential vegetation C stocks than Erb et al. (2018). However, present-day vegetation C stocks for S_{HNFull}, and $S_{HNCdens}$ are consistent with their values.

5. Conclusions

We conclude that differences between **BLUE** and **HN2017** arise from the higher allocation of cleared and harvested material to quickly decomposing pools in **BLUE**, compared to **HN2017**, combined with higher emissions in **BLUE** due to often larger

differences in soil and vegetation C densities between natural and managed vegetation or primary and secondary vegetation. It should be noted however that specific transitions and prevalence of specific PFTs in certain regions prohibits generalizing this statement. Together with the larger land-use dynamics which stem from **BLUE** representing gross transitions and its usage of LUH2v2.1 as LUC forcing, these changes lead to overall higher carbon losses that have a faster decay.

The two reference datasets of global C stocks seem to support the choice of C densities used in the default **BLUE** configuration and, therefore, the higher estimates of F_{LUC} by BLUE. However, it should be noted that both models have limited representation of spatial variability in C densities: **BLUE** ignores spatial variability in vegetation and soil C within each PFT distribution, for example due to less favorable climate in some regions; **HN2017** includes country-specific C densities for vegetation but not for soil, and no spatial variability within each country.

The large contribution of the C densities to the differences between the F_{LUC} estimates of the two BK models found in our results highlights the importance to derive spatially explicit maps of vegetation and soil C densities discriminated per vegetation type would be required. Producing such maps is challenging, especially for the estimates of C densities in undisturbed land, as most of the land surface has been directly or indirectly impacted by human activity. However, observation-based maps of vegetation and soil C densities in both disturbed and undisturbed land would be highly valuable, as they could be used in BK models to reduce uncertainties in F_{LUC}.

Similarly, improvements in allocation can be performed. Bookkeeping models, and many DGVMs, follow very simple assumptions of the fate of cleared or harvested material, often along the lines of the "Grand Slam Protocol" (McGuire et al., 2001), but developed for bookkeeping models earlier (Houghton et al., 1983), which distinguishes only three product pools (fast, medium, slow), with timescales defined rather ad-hoc as 1, 10, 100 years. The fractions going into these and into slash are compiled from individual studies for specific regions (Houghton et al., 1983; Hurtt et al., 2020), but are hard to quantify on the global level throughout several centuries. Such long timescales are needed, however, to capture the slow dynamics of decay and regrowth and thus to capture legacy fluxes accurately. For the last decades, however, more detailed data has become available than that currently used in the models of the Global Carbon Budgets, such as global sets of dynamic carbon-storage factors (Earles et al., 2012) that define a larger number of product pools and time-varying fractions of allocation.

Acknowledgements

We thank Andrea Castanho and Alexander A. Nassikas for support in extracting parameters from the HN2017 model.

References

Anav, A., Friedlingstein, P., Kidston, M., Bopp, L., Ciais, P., Cox, P., Jones, C., Jung, M., Myneni, R., and Zhu, Z.: Evaluating the Land and Ocean Components of the Global Carbon Cycle in the CMIP5 Earth System Models, 26, 6801–6843, https://doi.org/10.1175/JCLI-D-12-00417.1, 2013.

Arneth, A., Sitch, S., Pongratz, J., Stocker, B., Ciais, P., Poulter, B., Bayer, A., Bondeau, A., Calle, L., Chini, L., and others: Historical carbon dioxide emissions caused by land-use changes are possibly larger than assumed, 10, 79, 2017.

Bastos, A., Ciais, P., Barichivich, J., Bopp, L., Brovkin, V., Gasser, T., Peng, S., Pongratz, J., Viovy, N., and Trudinger, C. M.: Re-evaluating the 1940s CO_2 plateau, 13, 4877–4897, https://doi.org/10.5194/bg-13-4877-2016, 2016.

Bastos, A., O'Sullivan, M., Ciais, P., Makowski, D., Sitch, S., Friedlingstein, P., Chevallier, F., Rödenbeck, C., Pongratz, J., and Luijkx, I.: Sources of uncertainty in regional and global terrestrial CO2-exchange estimates, Global Biogeochemical Cycles, 2020.

Bayer, A. D., Lindeskog, M., Pugh, T. A. M., Anthoni, P. M., Fuchs, R., and Arneth, A.: Uncertainties in the land-use flux resulting from land-use change reconstructions and gross land transitions, 8, 91–111, https://doi.org/10.5194/esd-8-91-2017, 2017.

Brown, S. and Lugo, A. E.: The Storage and Production of Organic Matter in Tropical Forests and Their Role in the Global Carbon Cycle, 14, 161–187, https://doi.org/10.2307/2388024, 1982.

Erb, K.-H., Kastner, T., Plutzar, C., Bais, A. L. S., Carvalhais, N., Fetzel, T., Gingrich, S., Haberl, H., Lauk, C., Niedertscheider, M., Pongratz, J., Thurner, M., and Luyssaert, S.: Unexpectedly large impact of forest management and grazing on global vegetation biomass, Nature, 553, 73–76, https://doi.org/10.1038/nature25138, 2018.

FAO: Global Forest Resources Assessment 2015 (FRA2015), Food and Agriculture Organization of the United Nations, Rome, 2015.

FAOSTAT: FAOSTAT: Food and Agriculture Organization of the United Nations, Rome, Italy, 2015.

Friedlingstein, P., Jones, M., O'Sullivan, M., Andrew, R., Hauck, J., Peters, G., Peters, W., Pongratz, J., Sitch, S., and Le Quéré, C.: Global carbon budget 2019, Earth System Science Data, 11, 1783–1838, 2019.

Fuchs, R., Herold, M., Verburg, P. H., Clevers, J. G. P. W., and Eberle, J.: Gross changes in reconstructions of historic land cover/use for Europe between 1900 and 2010, 21, 299–313, https://doi.org/10.1111/gcb.12714, 2015.

Gasser, T. and Ciais, P.: A theoretical framework for the net land-to-atmosphere CO_2 flux and its implications in the definition of "emissions from land-use change," 4, 171–186, https://doi.org/10.5194/esd-4-171-2013, 2013.

Gasser, T., Crepin, L., Quilcaille, Y., Houghton, R. A., Ciais, P., and Obersteiner, M.: Historical CO 2 emissions from land use and land cover change and their uncertainty, Biogeosciences, 17, 4075–4101, 2020.

Grassi, G., House, J., Kurz, W. A., Cescatti, A., Houghton, R. A., Peters, G. P., Sanz, M. J., Viñas, R. A., Alkama, R., Arneth, A., Bondeau, A., Dentener, F., Fader, M., Federici, S., Friedlingstein, P., Jain, A. K., Kato, E., Koven, C. D., Lee, D., Nabel, J. E. M. S., Nassikas, A. A., Perugini, L., Rossi, S., Sitch, S., Viovy, N., Wiltshire, A., and Zaehle, S.: Reconciling global-model estimates and country reporting of anthropogenic forest CO2 sinks, 8, 914–920, https://doi.org/10.1038/s41558-018-0283-x, 2018.

Hansis, E., Davis, S. J., and Pongratz, J.: Relevance of methodological choices for accounting of land use change carbon fluxes, n/a–n/a, https://doi.org/10.1002/2014GB004997, 2015.

Hartung, K., Bastos, A., Chini, L., Ganzenmüller, R., Havermann, F., Hurtt, G. C., Loughran, T., Nabel, J. E. M. S., Nützel, T., Obermeier, W. A., and Pongratz, J.: Net land-use change carbon flux estimates and sensitivities – An assessment with a bookkeeping model based on CMIP6 forcing, 1–34, https://doi.org/10.5194/esd-2020-94, 2021.

Heinimann, A., Mertz, O., Frolking, S., Christensen, A. E., Hurni, K., Sedano, F., Chini, L. P., Sahajpal, R., Hansen, M., and Hurtt, G.: A global view of shifting cultivation: Recent, current, and future extent, 12, e0184479, 2017.

Hooijer, A., Page, S., Canadell, J. G., Silvius, M., Kwadijk, J., Wösten, H., and Jauhiainen, J.: Current and future CO_2 emissions from drained peatlands in Southeast Asia, 7, 1505–1514, https://doi.org/10.5194/bg-7-1505-2010, 2010.

460   Houghton, R. and Nassikas, A. A.: Global and regional fluxes of carbon from land use and land cover change 1850–2015, 31, 456–472, 2017.

Houghton, R., Hobbie, J., Melillo, J. M., Moore, B., Peterson, B., Shaver, G., and Woodwell, G.: Changes in the Carbon Content of Terrestrial Biota and Soils between 1860 and 1980: A Net Release of CO" 2 to the Atmosphere, 53, 235–262, 1983.

Houghton, R. A.: Terrestrial Fluxes of Carbon in GCP Carbon Budgets, Global Change Biology, 2020.

465   Houghton, R. A., House, J. I., Pongratz, J., van der Werf, G. R., DeFries, R. S., Hansen, M. C., Le Quéré, C., and Ramankutty, N.: Carbon emissions from land use and land-cover change, 9, 5125–5142, https://doi.org/10.5194/bg-9-5125-2012, 2012.

Hurtt, G. C., Chini, L., Sahajpal, R., Frolking, S., Bodirsky, B. L., Calvin, K., Doelman, J. C., Fisk, J., Fujimori, S., Goldewijk, K. K., Hasegawa, T., Havlik, P., Heinimann, A., Humpenöder, F., Jungclaus, J., Kaplan, J., Kennedy, J.,
470   Kristzin, T., Lawrence, D., Lawrence, P., Ma, L., Mertz, O., Pongratz, J., Popp, A., Poulter, B., Riahi, K., Shevliakova, E., Stehfest, E., Thornton, P., Tubiello, F. N., Vuuren, D. P. van, and Zhang, X.: Harmonization of Global Land-Use Change and Management for the Period 850–2100 (LUH2) for CMIP6, 1–65, https://doi.org/10.5194/gmd-2019-360, 2020.

Klein Goldewijk, K., Beusen, A., Doelman, J., and Stehfest, E.: New anthropogenic land use estimates for the Holocene: HYDE 3.2, Earth System Science Data, 9, 927–953, 2017.

475   Le Quéré, C., Andrew, R. M., Friedlingstein, P., Sitch, S., Pongratz, J., Manning, A. C., Korsbakken, J. I., Peters, G. P., Canadell, J. G., Jackson, R. B., and others: Global carbon budget 2017, 10, 405, 2018a.

Le Quéré, C., Andrew, R. M., Friedlingstein, P., Sitch, S., Hauck, J., Pongratz, J., Pickers, P. A., Korsbakken, J. I., Peters, G. P., Canadell, J. G., Arneth, A., Arora, V. K., Barbero, L., Bastos, A., Bopp, L., Chevallier, F., Chini, L. P., Ciais, P., Doney, S. C., Gkritzalis, T., Goll, D. S., Harris, I., Haverd, V., Hoffman, F. M., Hoppema, M., Houghton, R. A., Hurtt, G., Ilyina, T.,
480   Jain, A. K., Johannessen, T., Jones, C. D., Kato, E., Keeling, R. F., Goldewijk, K. K., Landschützer, P., Lefèvre, N., Lienert, S., Liu, Z., Lombardozzi, D., Metzl, N., Munro, D. R., Nabel, J. E. M. S., Nakaoka, S.-I., Neill, C., Olsen, A., Ono, T., Patra, P., Peregon, A., Peters, W., Peylin, P., Pfeil, B., Pierrot, D., Poulter, B., Rehder, G., Resplandy, L., Robertson, E., Rocher, M., Rödenbeck, C., Schuster, U., Schwinger, J., Séférian, R., Skjelvan, I., Steinhoff, T., Sutton, A., Tans, P. P., Tian, H., Tilbrook, B., Tubiello, F. N., van der Laan-Luijkx, I. T., van der Werf, G. R., Viovy, N., Walker, A. P., Wiltshire, A. J.,
485   Wright, R., Zaehle, S., and Zheng, B.: Global Carbon Budget 2018, 10, 2141–2194, https://doi.org/10.5194/essd-10-2141-2018, 2018b.

Li, W., MacBean, N., Ciais, P., Defourny, P., Lamarche, C., Bontemps, S., Houghton, R. A., and Peng, S.: Gross and net land cover changes based on plant functional types derived from the annual ESA CCI land cover maps, 2018.

Pongratz, J., Reick, C., Raddatz, T., and Claussen, M.: Effects of anthropogenic land cover change on the carbon cycle of the
490   last millennium, Global Biogeochemical Cycles, 23, 2009.

Pongratz, J., Reick, C. H., Houghton, R., and House, J.: Terminology as a key uncertainty in net land use and land cover change carbon flux estimates, 5, 177–195, 2014.

Post, W. M., Emanuel, W. R., Zinke, P. J., and Stangenberger, A. G.: Soil carbon pools and world life zones, 298, 156–159, https://doi.org/10.1038/298156a0, 1982.

495   Pugh, T., Arneth, A., Olin, S., Ahlström, A., Bayer, A., Goldewijk, K. K., Lindeskog, M., and Schurgers, G.: Simulated carbon emissions from land-use change are substantially enhanced by accounting for agricultural management, Environmental Research Letters, 10, 124008, 2015.

Ramankutty, N. and Foley, J. A.: Estimating historical changes in global land cover: Croplands from 1700 to 1992, 13, 997–1027, 1999.

500   Schlesinger, W. H.: Soil Organic Matter: a Source of Atmospheric CO2, in: The Role of Terrestrial Vegetation in the Global Carbon Cycle: Measurement by Remote Sensing, 1984.

Shukla, P., Skeg, J., Buendia, E. C., Masson-Delmotte, V., Pörtner, H.-O., Roberts, D., Zhai, P., Slade, R., Connors, S., and van Diemen, S.: Climate Change and Land: an IPCC special report on climate change, desertification, land degradation, sustainable land management, food security, and greenhouse gas fluxes in terrestrial ecosystems, 2019.

505   Stocker, B. and Joos, F.: Quantifying differences in land use emission estimates implied by definition discrepancies, 2015.

Stocker, B., Strassmann, K., and Joos, F.: Sensitivity of Holocene atmospheric CO2 and the modern carbon budget to early human land use: analyses with a process-based model, Biogeosciences, 8, 69–88, 2011.

Van Der Werf, G., Randerson, J., Giglio, L., Van Leeuwen, T., Chen, Y., Rogers, B., Mu, M., Van Marle, M., Morton, D., Collatz, G., and others: Global fire emissions estimates during 1997–2016, Earth Syst. Sci. Data, 9, 697–720, 2017.

510   Vittorio, A. V. D., Shi, X., Bond-Lamberty, B., Calvin, K., and Jones, A.: Initial Land Use/Cover Distribution Substantially Affects Global Carbon and Local Temperature Projections in the Integrated Earth System Model, 34, e2019GB006383, https://doi.org/10.1029/2019GB006383, 2020.

Wilkenskjeld, S., Kloster, S., Pongratz, J., Raddatz, T., and Reick, C. H.: Comparing the influence of net and gross anthropogenic land-use and land-cover changes on the carbon cycle in the MPI-ESM, 11, 4817–4828, 2014.

515   Zinke, P. J., Millemann, R. E., and Boden, T. A.: Worldwide organic soil carbon and nitrogen data, Carbon Dioxide Information Center, Environmental Sciences Division, Oak …, 1986.

520

525

Appendix A

Table A1 – Plant functional types in HN2017 and in BLUE, and the correspondence used in this study.

HN2017	BLUE
Tropical Rainforest	Tropical evergreen forest
Tropical Moist Deciduous	Tropical deciduous forest
Tropical Dry Forest	
Tropical Shrub	Raingreen shrubs
Tropical Desert	
Tropical Mountain	Tropical evergreen forest
Subtropical Humid Forest	Temperate evergreen broadleaf forest
Subtropical Dry Forest	Temperate/boreal deciduous broadleaf forest
Subtropical Steppe	C4 natural grasses
Subtropical Desert	
Subtropical Mountain	Temperate/boreal evergreen conifers
Temperate Oceanic	Temperate/boreal evergreen conifers
Temperate continental	Temperate/boreal deciduous broadleaf forest
Temperate steppe	C3 natural grasses
Temperate Desert	
Temperate Mountain	Temperate/boreal deciduous broadleaf forest
Boreal Coniferous	Temperate/boreal evergreen conifers
Boreal Tundra	Tundra
Boreal Mountain	
Polar	Tundra

Table A2 – Global median value across countries per PFT for vegetation C densities and PFT-dependent soil C densities from BLUE, and from HN2017 converted to BLUE PFT classes as used for the simulations with parameters from HN2017. Units are tC/ha.

	Primary Veg C		Secondary Veg C		Pasture Veg C		Crop Veg C		Primary Soil C		Secondary Soil C		Pasture Soil C		Crop Soil C	
	BLUE	HN2017	BLUE	HN2017	BLUE	HN2017	BLUE	HN2017	BLUE	HN2017	BLUE	HN2017	BLUE	HN2017	BLUE	HN2017
Tropical evergreen forest	200	152	150	114	18	10	5	5	117	98	88	88	88	98	58	73
Tropical deciduous forest	160	92	120	69	18	10	5	5	117	100	88	90	88	100	58	75
Temperate evergreen broadleaf forest	160	138	120	103	7	10	5	5	134	120	120	108	101	120	67	90
Temperate/boreal deciduous broadleaf forest	135	86	100	64	7	10	5	5	134	143	120	129	101	143	67	108
Temperate/boreal evergreen conifers	90	110	68	83	7	10	5	5	206	182	185	164	155	182	103	137
Temperate/boreal deciduous conifers	90	110	68	83	7	10	5	5	206	182	185	164	155	182	103	137
Raingreen shrubs	27	37	27	28	18	10	5	5	69	35	69	32	69	35	34	26
Summergreen shrubs	27	37	27	28	7	10	5	5	69	35	69	32	69	35	34	26
C3 natural grasses	7	23	7	17	7	10	5	3	189	80	189	72	189	80	94	60
C4 natural grasses	18	23	18	17	18	10	5	5	42	50	42	45	42	50	21	38
Tundra	3	14	0	11	7	7	1	5	204	178	204	160	204	178	101	134

Table A3 – Global median values of harvest and clearing allocation rules to the short-, medium- and long-lived pools (1, 10 and 100 years) for BLUE PFTs, from the standard BLUE setup and used for the simulations with parameters from HN2017 (converted to BLUE PFT classes). The slash fraction from clearing is calculated as the 1 minus the sum of the 1-, 10- and 100-year pools.

	Slash Primary Forest		Slash Secondary Forest		Harvest Pool 1		Harvest Pool 10		Harvest Pool 100		Clearing Pool 1		Clearing Pool 10		Clearing Pool 100	
	BLUE	HN2017	BLUE	HN2017	BLUE	HN2017	BLUE	HN2017	BLUE	HN2017	BLUE	HN2017	BLUE	HN2017	BLUE	HN2017
Tropical evergreen forest	0.79	0.5	0.71	0.5	0.90	0.49	0.04	0.11	0.06	0.40	0.4	0.42	0.27	0.01	0	0.08
Tropical deciduous forest	0.86	0.5	0.81	0.5	0.90	0.49	0.04	0.11	0.06	0.40	0.4	0.42	0.27	0.01	0	0.08
Temperate evergreen broadleaf forest	0.81	0.5	0.75	0.5	0.40	0.49	0.24	0.11	0.36	0.40	0.4	0.42	0.2	0.01	0.07	0.08
Temperate/boreal deciduous broadleaf forest	0.78	0.5	0.7	0.5	0.40	0.49	0.24	0.11	0.36	0.40	0.4	0.42	0.2	0.01	0.07	0.08
Temperate/boreal evergreen conifers	0.87	0.5	0.82	0.5	0.40	0.49	0.24	0.11	0.36	0.40	0.4	0.42	0.2	0.01	0.07	0.08
Temperate/boreal deciduous conifers	0.87	0.5	0.82	0.5	0.40	0.49	0.24	0.11	0.36	0.40	0.4	0.42	0.2	0.01	0.07	0.08
Raingreen shrubs	0.86	0.5	0.81	0.5	1.00	0.49	0.00	0.11	0.00	0.40	0.4	0.42	0.1	0.01	0	0.08
Summergreen shrubs	0.78	0.5	0.7	0.5	1.00	0.49	0.00	0.11	0.00	0.40	0.4	0.42	0.1	0.01	0	0.08
C3 natural grasses	0.78	0.5	0.7	0.5	1.00	0.49	0.00	0.11	0.00	0.40	0.5	0.42	0	0.01	0	0.08
C4 natural grasses	0.86	0.5	0.81	0.5	1.00	0.49	0.00	0.11	0.00	0.40	0.5	0.42	0	0.01	0	0.08
Tundra	0.87	0.5	0.82	0.5	1.00	0.49	0.00	0.11	0.00	0.40	0.42	0.4	0.01	0.1	0.08	0

565
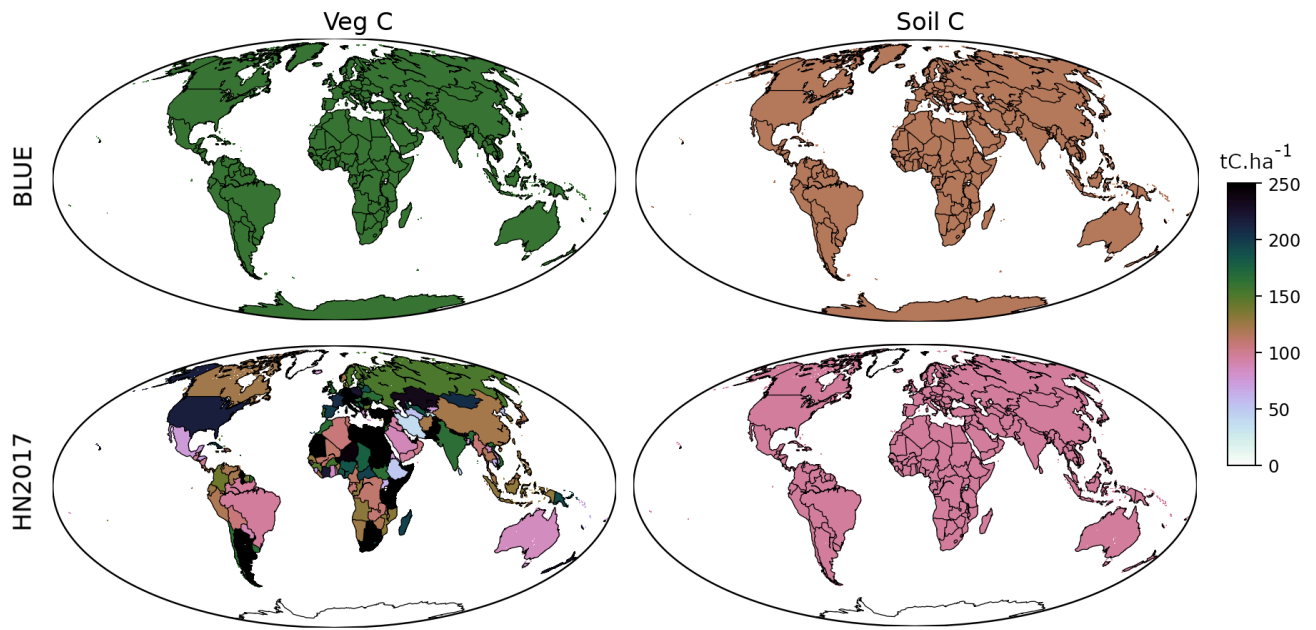
Figure A1 – Carbon densities in vegetation (left) and soil (right) for Tropical Broadleaved Evergreen forests for BLUE (top) and HN2017 (bottom) in tC.ha^{-1} . It should be noted that even though C density values are assigned on a per-country basis in HN2017, they do not differ between countries for soil C. Note that C densities are assigned to all countries, even if evergreen broadleaved forest is not present in a given country.